Feasibility study of focal lens for multistatic microwave breast imaging

Daniela M. Godinho
Instituto de Biofísica e Engenharia Biomédica
Faculdade de Ciências da Universidade de Lisboa
Lisboa, Portugal
dgodinho94@gmail.com

João M. Felício
Instituto de Telecomunicações
Instituto Superior Técnico, Universidade de Lisboa
Lisboa, Portugal
joao.felicio@lx.it.pt

Carlos A. Fernandes
Instituto de Telecomunicações
Instituto Superior Técnico, Universidade de Lisboa
Lisboa, Portugal
carlos.fernandes@lx.it.pt

Raquel C. Conceição
Instituto de Biofísica e Engenharia Biomédica
Faculdade de Ciências da Universidade de Lisboa
Lisboa, Portugal
raquelcruzconceicao@gmail.com

Abstract—**Microwave Imaging is an emerging technique to aid breast cancer diagnosis. Current multistatic setups involve complex and heavy signal processing techniques, such as to remove the energy coupling between adjacent sensors, which masks the response from inner tissues. We investigate a novel approach using a dielectric lens in order to reduce the coupling effects between antennas, thus reducing the signal processing burden, while preserving all the advantages of multistatic setups. In this paper, we show that we can successfully detect simulated breast targets on reconstructed images using a setup with a dielectric lens.**

Keywords—Bessel beam, breast cancer detection, dielectric lens, focusing lens, microwave imaging, multistatic setup.

I. INTRODUCTION

In 2018, 2.09 million new breast cancer cases were reported worldwide, being the second most common cancer after lung cancer [1]. Microwave Imaging (MWI) has been studied as a possible new imaging technique to aid breast cancer diagnosis, which has several advantages when compared to the currently used imaging techniques. It uses non-ionising radiation, it does not require breast compression, it uses low power and it is relatively low-cost [2].

Ultra-Wide Band Radar (UWB) is one of the techniques of MWI which has been proposed to image the breast. One or more antennas will transmit a UWB pulse, illuminating the breast, and they will record its backscattered signals. These scattered signals are used to create an intensity profile of the breast using reconstruction algorithms. High energy regions of the image will correspond to the detection of potential tumors [3].

MWI systems can be monostatic or multistatic. In a monostatic configuration the signals are transmitted and received by the same antenna, while in a multistatic configuration one antenna transmits the radar signal, and the remaining antennas record the scattered echoes. Both configurations have been used in several prototypes by different groups working in breast microwave imaging. Monostatic systems usually use only one antenna to scan the breast resulting in long acquisition times, while multistatic systems require less time as they scan the breast with multiple antennas simultaneously, at the expense of more complex signal processing algorithms due to coupling effects between antennas. Another advantage of using multistatic systems is the possibility to use power amplifiers in order to increase the dynamic range, which is important in situations where the target can have a low response.

At the University of Calgary, Fear *et al.* developed a prototype for a study with patients using a monostatic system, where a UWB antenna was moved across 200 positions, taking around 30 minutes to perform a full breast exam [4]. Xie *et al.* [5] presented results from simulations of a multistatic system with 72 antennas and the algorithms to process the obtained signals. MVG Industries [6] have used a breast imaging system for human patient studies with a multistatic setup of 18 antennas resulting in a scan time of 10 minutes. Klemm *et al.* [7], from University of Bristol, presented a new prototype with 60 antennas in a multistatic system which was capable of performing all measurements in 10 seconds.

In this paper, we study the feasibility of a multistatic system that uses a Bessel lens antenna to produce a pencil beam illumination of the breast, thus decreasing the coupling effects with the antennas distributed around the breast. This system topology should reduce the signal processing burden involved in multistatic systems, while enabling the use of a power amplifier at the feed antenna and increasing the robustness of the setup to noise. This is an important feature explored here, as one of our goals is to use dry imaging setups. In a dry imaging setup the antennas and the breast are placed in air, without the immersion medium between them as is commonly proposed in other MWI setups [6, 8].

In 2007, Wang *et al.* [9] used a flat left-handed metamaterial lens to study the focusing properties of microwave detection and imaging of targets in free space. Akhter *et al.* [10] presented a Vivaldi antenna and a hemispheric dielectric lens in a monostatic setup to improve the detection of metallic targets, which could be applied to illegal imports detection. To the best of our knowledge, using lenses for medical MWI has never been attempted before.

II. SETUP UNDER INVESTIGATION

This section summarises the simulated setup, as well as the antenna and the dielectric lens used to study the system topology. All these elements were designed and

simulated using the Computer Simulation Technology (CST) Studio software [11].

A. Setup

Our setup was designed for a scenario in which the patient lies in prone position, with the breast extending through an opening on the table. It is a bistatic configuration where a ring of antennas, or a single antenna rotating around the breast is positioned in the same z-plane (Fig. 1). The breast is simulated as a sphere in this study. The lens with the respective feed is placed below the breast, using its pencil beam to focus in specific regions, thus decreasing the coupling effect with the surrounding antennas. In contrast with other MWI prototypes, a coupling medium is not used in this setup. It can be shown that the resulting contrast at the air/skin interface does not penalise excessively the amplitude of the tumour scattered signals, provided that proper signal processing is used for artefact removal [12]. This includes detailed knowledge of the breast shape, which can be obtained with a very low-cost optical system (e.g. a webcam).

Our setup was first simulated in free-space and then in the presence of the simplified breast phantom (the sphere) with embedded metallic spherical targets. The breast was mimicked by a dielectric sphere of 50 mm radius, with a material with a loss tangent of 0.1, and a constant value of real permittivity over frequency, $\varepsilon_r = 8$, which corresponds to the upper limit of fat permittivity [13]. Although real breast tissues are not homogeneous, it was demonstrated in [11] that an appropriate average of the permittivity of fat and fibroglandular tissues is enough for clear tumour imaging. On the other hand, we intentionally use a simplified version of the breast in the present study, to test the feasibility of this type of setup without introducing additional confounders. In future tests, a more complex phantom will be considered. Two Perfect Electric Conductor (PEC) spheres of 5 mm radius were considered as targets, placed at $x = 30$ mm and $x = -30$ mm, respectively, from the centre of the dielectric sphere.

For the purpose of this study, we considered only a bistatic topology, although the conclusions may be extended to multistatic systems. In this sense, two Linearly Polarised (LP) antennas were included in the numerical setup: one feed with a lens and one feed rotating in the *xy*-plane around the dielectric sphere in a total of twelve positions (30º degrees step) at constant distance of 30 mm from the air-dielectric interface. In order to ensure polarisation match between the LP transmit (Tx) and the receive (Rx) antennas, we synchronously rotated the Tx antenna as the Rx antenna swept the dielectric sphere.

A distance greater than 100 mm from the feed behind the lens to the phantom was required in order to create a narrow pencil beam. A comparable setup without the lens was also simulated in order to study the consequences of having such great distance between the feed and the phantom. The antenna was placed at a distance from the breast phantom equivalent to the distance considered in the setup with the "feed + lens", which was found ensuring both setups had the same electric field intensity at the surface of the phantom.

B. Antenna

For the purpose of this study, we opted for a planar slot-based single-layer printed antenna introduced in [14]. It is formed by two crossed exponential slots, balance fed between two metallisation edges (see Fig. 2). The main advantages of this configuration are the highly stable radiation pattern and phase centre, as well as very pure linear polarisation along the entire bandwidth. The XETS was designed to be impedance-matched from 2 to 6 GHz (Fig. 3). Its final design, illustrated in Fig. 2, is quite compact, with 28 mm radius.

The XETS was used both as a stand-alone pick-up antenna around the dielectric sphere, and as the primary feed of the dielectric lens. We chose to use a Bessel lens, because it produces a pencil beam in the near-field, with near constant radius along the lens axis. This allows a good spatial selectivity of the illuminated region. The lens is axial-symmetric, and was designed, using Geometrical

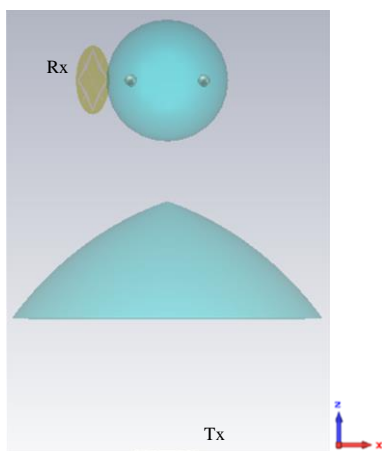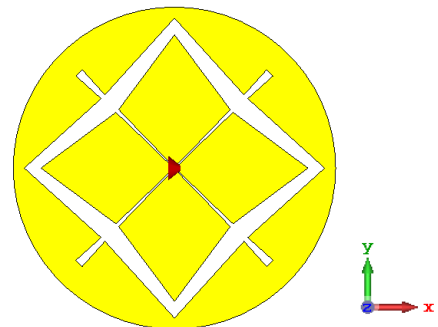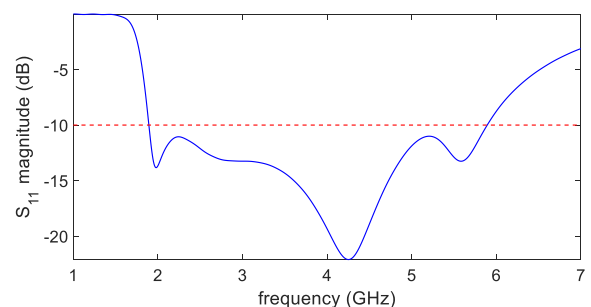Fig. 2. XETS antenna used to study the system topology.

Fig. 1. Schematic of the setup presented in this paper. The feed below the lens and the lens comprise the transmit antenna (Tx), a sphere – mimicking the breast – with two targets is placed in front of the lens and an antenna (Rx) will rotate around them recording the receiving signal.

Fig. 3. Plot of the magnitude in dB of the reflection coefficient parameter (s_{11}) of the XETS antenna over frequency.

Optics, to have continuous focus along the axis. This condition implies a plane wave front in the main near-field beam. The dielectric material is Polylactide Acid (PLA), which is a 3D-printable and has a dielectric constant of 2.9 and loss tangent of 0.013 [15]. The lens has around 250 mm diameter and 95 mm depth.

III. IMAGE RECONSTRUCTION ALGORITHM

The algorithm used for image reconstruction was based on the wave migration algorithm [16], where the intensity of each pixel is calculated considering the distances between each antenna position and each voxel (Fig. 4), with the following equation:

$$intensity(p) = \sum_{i,j}^{N_a} \sum_{f_k}^{N} s_{ij}(f_k)\, e^{jk_0(d_{in} + n_{diel}\, d_{diel} + d_{out})}$$

where d_{in} is an equivalent electric distance between the XETS and the entry plane of the sphere, taking into account the electric length of the XETS and the lens. d_{diel} is the distance from the entry point to voxel p plus the distance from the voxel to the exit point of the sphere, and n_{diel} is the dielectric refractive index. Distance d_{out} is the remaining distance up to the receive antenna. N_a is the number of antennas, s_{ij} is the calibrated scattering matrix element between the i-th and j-th antennas, with dimension $1 \times N$, where N is the number of frequency points, and $k_0 = \frac{2\pi f(f_k)}{c}$ is the free-space wavenumber at frequency f_k with c as the speed of light. It can be shown that refraction effects are not significant in this configuration, therefore these were ignored in the image reconstruction algorithm.

For now, an ideal calibration was considered, meaning that $s_{ij}(f_k)$ is the difference between the simulated response from all components of the setup (lens system, breast and PEC targets) and the simulated response of the same setup without the targets.

IV. RESULTS

This section presents the results obtained with the setup described in Section II.

A. Bessel lens near-fields

To assess the suitability of the dielectric lens, we simulated the electric field of the standalone "feed + lens" over the entire bandwidth of 2-6 GHz. Fig. 5 shows the magnitude of electric field over the xz-plane.
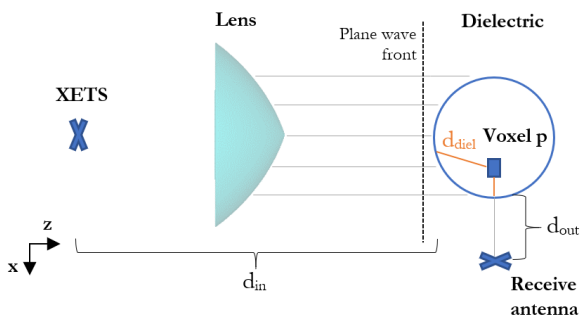

Fig. 4. Schematic of the considered distances in the image reconstruction algorithm.
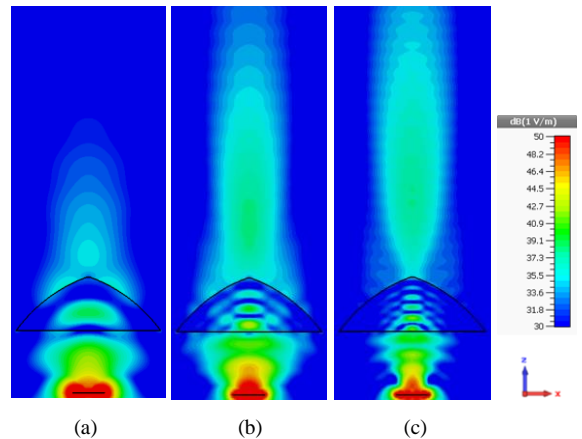

(a) (b) (c)

Fig. 5. Electric field map in the near-field of the XETS antenna as the feed of the Bessel lens. Different frequencies are depicted in the figure: (a) 2 GHz, (b) 4 GHz and (c) 6 GHz.

At 2 GHz, the focused energy is somewhat limited. This is a consequence of the large wavelength ($\lambda_{2GHz} = 15$ mm) compared to the physical dimension of the lens. This effect could be mitigated by increasing the size of the lens, at the expense of larger weight and cost of the overall setup. Yet, we found that the current dimensions offered a good trade-off between these variables. As for higher frequencies, it is possible to observe that the Bessel lens creates a narrower beam which extends along the z-direction, thus proving that the lens can be used to focus energy into the breast.

B. Transmission signals

We recorded the transmission coefficients between Tx and Rx antennas. As an example, Fig. 6 shows the s_{ij} of the targets response obtained in CST simulation for the twelve positions of the Rx antenna for both setups with and without lens. Some s_{ij} signals overlap due to existing setup symmetries. The level of the targets response in both setups is similar, below −40 dB, which means that adding a lens to the setup and increasing the distance between the feed and the targets do not produce a significant reduction in the targets response.

The transmitted power is 0 dBm, while all received signals are above −80 dBm within the proposed frequency band of 2-6 GHz, i.e., they are above the noise level of our equipment which is −110 dBm [12]. Increasing the difference between the signal level and noise level is of great importance and is possible in this bistatic setup by using a power amplifier at the Tx or at the Rx end.

C. Reconstructed images

Fig. 7 shows the obtained reconstructed images in xz and xy planes. The color code corresponds to the intensity of the reflected signals, with the lighter colors corresponding to higher intensities. The actual positions of the target are marked in red. Both targets were successfully detected, although with a rather elongated shape in the xz-plane. This is due to lack of vertical diversity of antenna planes (only one z-plane was considered).
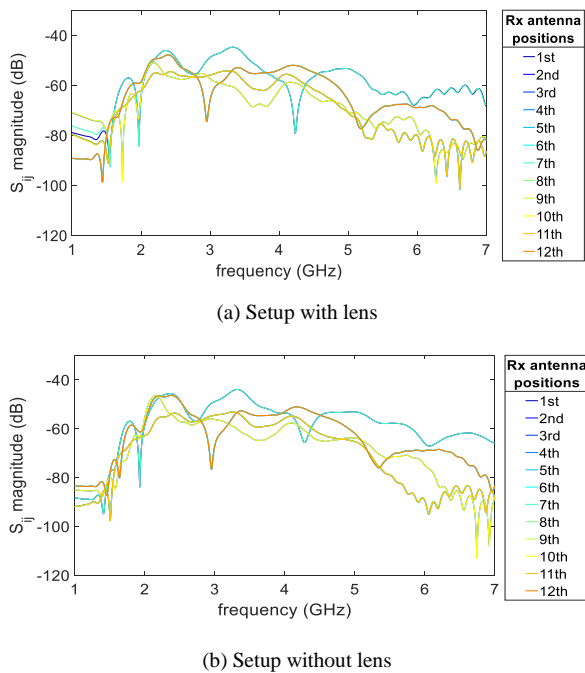
(a) Setup with lens

(b) Setup without lens

Fig. 6. Plots of the magnitude in dB of transmission coefficients (s_{ij}) between Tx and Rx antennas, corresponding to the targets response in (a) a setup with lens and in (b) a setup without lens.
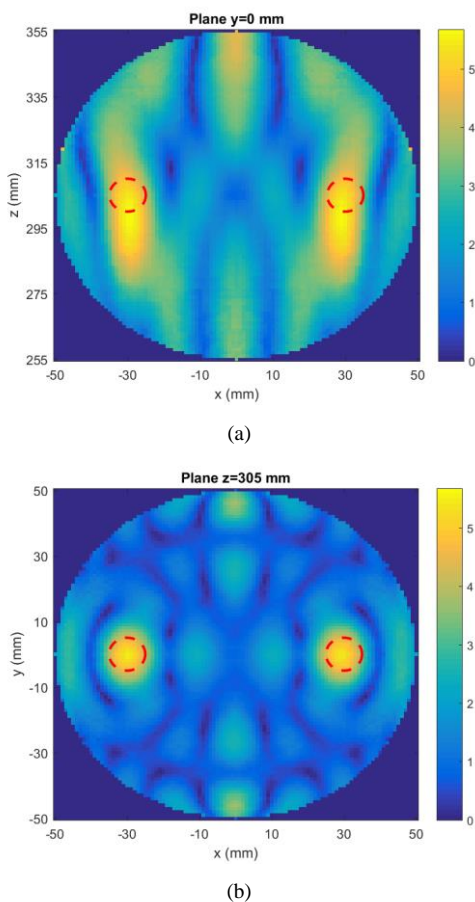

(a)

(b)

Fig. 7. Reconstructed images of the dielectric sphere with two targets. *xz* plane and *xy* plane are represented in (a) and (b), respectively. The red dashed circles correspond to the actual location and shape of the targets.

V. CONCLUSIONS

Our results showed that by using the Bessel lens we can illuminate the dielectric sphere with a pencil beam and reconstruct the image with a satisfactory result, detecting both targets.

In the future, the reduction of the coupling effects between antennas will be studied. A larger comparison using the same setup without the lens will also be addressed, as well the study of the Specific Absorption Rate (SAR) for both setups. We will proceed to the fabrication of the lens and the experimental validation of this setup. In order to be able to test a realistic situation where the targets cannot be removed, the implementation of an artefact removal algorithm is also required. A more complex phantom will also be tested, considering an anthropomorphic shape, inserting fibroglandular tissue and skin, while mimicking the tissues with state-of-the-art dielectric properties. The introduction of an alternative circular polarisation feed for the lens can also be explored, so as to avoid polarisation matching issues between Tx and Rx antennas.

REFERENCES

[1] International Agency for Research on Cancer - World Health Organization. (2018, 11/04/2019). GLOBOCAN 2018: Estimated Cancer Incidence, Mortality and Prevalence Worldwide in 2018 - Cancer Fact Sheets. Available: http://gco.iarc.fr/today/fact-sheets-cancers

[2] R. C. Conceição, M. O'Halloran, M. Glavin, and E. Jones, "Comparison of Planar and Circular Antenna Configurations For Breast Cancer Detection Using Microwave Imaging," Progress In Electromagnetics Research, vol. 99, pp. 1-20, 2009.

[3] H. B. Lim, N. T. T. Nhung, E. Li, and N. D. Thang, "Confocal Microwave Imaging for Breast Cancer Detection: Delay-Multiply-And-Sum Image Reconstruction Algorithm," IEEE Transactions on Biomedical Engineering, vol. 55, no. 6, pp. 1697-1704, 2008.

[4] E. C. Fear, J. Bourqui, C. Curtis, D. Mew, B. Docktor, and C. Romano, "Microwave breast imaging with a monostatic radar-based system: A study of application to patients," IEEE Transactions on Microwave Theory and Techniques, vol. 61, no. 5, pp. 2119-2128, 2013.

[5] Y. Xie, B. Guo, L. Xu, J. Li, and P. Stoica, "Multistatic Adaptive Microwave Imaging for Early Breast Cancer Detection," IEEE Transactions on Biomedical Engineering, vol. 53, no. 8, pp. 1647-1657, 2006.

[6] A. Fasoula, L. Duchesne, J. D. G. Cano, P. Lawrence, G. Robin, and J. G. Bernard, "On-Site Validation of a Microwave Breast Imaging System, before First Patient Study," Diagnostics, vol. 8, no. 3, 53, pp. 1-38, 2018.

[7] M. Klemm et al., "Development and Testing of a 60-Element UWB Conformal Array for Breast Cancer Imaging," in Proceedings of the 5th European Conference on Antennas and Propagation (EUCAP), Rome, Italy, 2011.

[8] A. W. Preece, I. Craddock, M. Shere, L. Jones, and H. L. Winton, "MARIA M4: clinical evaluation of a prototype ultrawideband radar scanner for breast cancer detection," Journal of Medical Imaging, vol. 3, no. 3, 2016.

[9] G. Wang, J. Fang, and X. Dong, "Resolution of Near-Field Microwave Target Detection and Imaging by Using Flat LHM Lens," IEEE Transactions on Antennas and Propagation, vol. 55, no. 12, pp. 3534-3541, 2007.

[10] Z. Akhter, B. N. Abhijith, and M. J. Akhtar, "Hemisphere lens-loaded Vivaldi antenna for time domain microwave imaging of concealed objects," Journal of Electromagnetic Waves and Applications, vol. 30, no. 9, pp. 1183-1197, 2016.

[11] CST – Computer Simulation Technology. Available: https://www.cst.com/

[12] J. M. Felício, J. M. Bioucas-Dias, J. R. Costa, and C. A. Fernandes, "Microwave Breast Imaging using a Dry Setup," IEEE Transactions on Computational Imaging (in press) pp. 1-15, 2019.

[13] M. Lazebnik et al., "A Large-Scale Study of the Ultrawideband Microwave Dielectric Properties of Normal, Benign and Malignant Breast Tissues Obtained from Cancer Surgeries," Physics in Medicine and Biology, vol. 52, pp. 6093–6115, 2007.

[14] J. R. Costa and C. A. Fernandes, "Broadband slot feed for integrated lens antennas," IEEE Antennas and Wireless Propagation Letters, vol. 6, 2007.

[15] J. M. Felício, C. A. Fernandes, and J. R. Costa, "Complex permittivity and anisotropy measurement of 3D-printed PLA at microwaves and millimeter-waves," in 2016 22nd International Conference on Applied Electromagnetics and Communications (ICECOM), Dubrovnik, Croatia, 2016, pp. 1-6.

[16] J. M. Lopez-Sanchez and J. Fortuny-Guasch, "3-D Radar Imaging Using Range Migration Techniques," IEEE Transactions on Antennas and Propagation, vol. 48, no. 5, pp. 728-737, 2000.